THE JOURNAL OF PHYSICAL CHEMISTRY B
A JOURNAL OF THE AMERICAN CHEMICAL SOCIETY

pubs.acs.org/JPCB

Article

Formation of β-U_3O_8 from UCl_3 Salt Compositions under Oxygen Exposure

Benjamin W. Tuffy,[#] Nancy R. Birkner,[#] Juliano Schorne-Pinto, Ryan C. Davis, Amir M. Mofrad, Clara M. Dixon, Mina Aziziha, Matthew S. Christian, Timothy J. Lynch, Maxwell T. Bartlett, Theodore M. Besmann, Kyle S. Brinkman, and Wilson K. S. Chiu*

Cite This: *J. Phys. Chem. B* 2024, 128, 11174–11185

Read Online

ACCESS | Metrics & More | Article Recommendations | Supporting Information

ABSTRACT: Complementary X-ray absorption fine structure (XAFS) and Raman spectroscopy studies were conducted on various UCl_3 concentrations in alkali chloride salt compositions. The samples were 5 mol % UCl_3 in LiCl (S1), 5 mol % UCl_3 in KCl (S2), 5 mol % UCl_3 in LiCl–KCl eutectic (S4), 50 mol % UCl_3 in KCl (S5), and 20 mol % UCl_3 in KCl (S6) molar concentrations. Samples were heated to 800 °C and allowed to cool to room temperature with measurements performed at selected temperatures; the highest temperatures showed the most stability and will be primarily referenced for conclusions. The processing and interpretation of the Raman and extended X-ray absorption fine structure (EXAFS) peaks revealed several uranium–oxygen bond lengths and symmetries in the samples before, during, and after heating. Based on published thermodynamic data of similar systems, X-ray absorption fine structure spectroscopy, and identification of Raman peaks, a β variation of α-U_3O_8, typical at room temperature, is the suspected dominant phase of all samples at high temperatures (800 °C). In the existing literature, this β structure of U_3O_8 was synthesized by slow cooling of uranium oxides from 1350 °C. This paper suggests the rapid formation of the compound due to the decomposition of the uranium chlorides or oxychlorides at increasing temperatures and O_2 reaction kinetics.

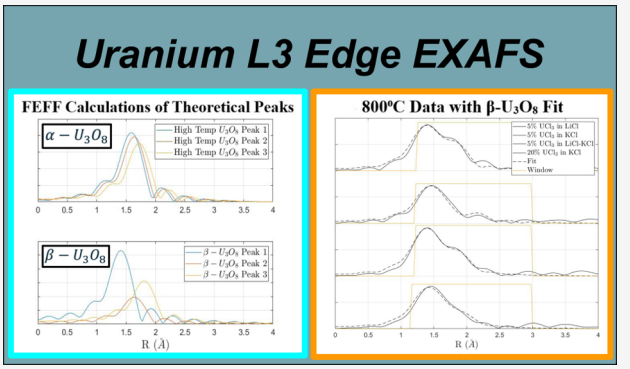

1. INTRODUCTION

In the Generation IV International forum, the concept of a molten salt reactor (MSR) re-emerged as one of the key concepts for the development of Gen IV nuclear reactors.[1,2] Success had already been shown in Oak Ridge National Lab's 1965 Molten Salt Reactor Experiment (MSRE). Higher operating temperatures and liquid coolant led to increased thermodynamic efficiencies and removed the need for a highly pressurized steam system. There is also potential to utilize previously spent fuels and achieve far higher burnup of all fuels. The concept of molten state fuel in the form of uranium chlorides brings about a host of safety benefits but requires new physical insights and understanding. As with any new concept, especially those in the field of nuclear engineering and chemistry, a comprehensive understanding of the system and all its subsequent components, byproducts, and kinetics is essential to safety and success.

The original intent of this work was to identify the complex coordination states that occur when UCl_3 fuel salt exists in highly ionic LiCl and KCl molten salts. The need to identify structures, dynamic interactions in the ionic media, validating of computational models, determining of viscosity, and a host of other research were identified as necessary steps for MSR research.[1] Understanding experimentally the coordination, structure, and kinetics experienced by uranium in this media is invaluable for reactor physics.

This work would build on the existing literature related to UCl_3 salt compositions.[3−9] Okamoto et al.[3] successfully collected XAFS data of 15% mol UCl_3 in LiCl–KCl eutectic and reported a U–Cl bond length, U coordination number, and Debye–Waller factor. Several first-principles molecular dynamics (FPMD) studies have also been published for this composition, where for example, the U–U second coordination bond is calculated.[4,6,7] This work provides several different molar UCl_3 concentrations and several different LiCl/KCl salt compositions. If successful, this work would replicate Okamoto's data, build on it by identifying the second coordination U–U bond, and potentially identify variance in data between pure LiCl, pure KCl, and LiCl–KCl eutectic.

Received: April 29, 2024
Revised: October 21, 2024
Accepted: October 23, 2024
Published: November 5, 2024

https://doi.org/10.1021/acs.jpcb.4c02776
J. Phys. Chem. B 2024, 128, 11174–11185

Table 1. Sample Compositions Based on Targeted Weights and Actual Compositions Inferred from the ICP-OES Analysis

salt composition	values in mol %											
	theoretical			from weighting			from powders—ICP			extracted from Ni liners—ICP		
	LiCl	KCl	UCl3	LiCl	KCl	UCl3	LiCl	KCl	UCl3	LiCl	KCl	UCl3
S1:5 mol % UCl_3 in LiCl	95	0	5	94.76	0	5.24	95.35	0	4.65	95.44	0	4.56
S2:5 mol % UCl_3 in KCl	0	95	5	0	94.93	5.07	0	95.20	4.80	0	95.21	4.79
S4:5 mol % UCl_3 in LiCl-KCl	55.1	39.9	5	56.29	38.78	4.93	60.08	35.23	4.69			
S5:50 mol %UCl_3 in KCl	0	50	50	0	50.18	49.82	0	52.19	47.81	0	50.83	49.17
S6:20 mol %UCl_3 in KCl	0	80	20	0	80	20						

There is a computationally modeled, but not reported in *in situ* work, K_2UCl_5 ternary that would appear in potassium salts and not in pure lithium salts.

Despite samples being prepared with near pure UCl_3, by the time of data collection at SSRL's Beamline 11-2 (SLAC National Accelerator Laboratory, Stanford, California) and Raman measurements, almost all data showed abnormalities, which have since been resolved as oxygen contamination of the system. Some Raman spectra did show the existence initially of pure UCl_3. It is known that uranium metal is incredibly reactive with oxygen and that uranium chlorides in the presence of oxygen results in a complex uranium chloride, uranium oxide, and uranium oxychloride phase diagram.[10−12] At atmospheric oxygen concentrations, the system will trend toward a phase composition of UO_2, $UO_{2.x}$, and U_3O_8.[13] This holds even in the presence of chlorine that uranium oxides are still dominant at atmospheric quantities and pressures of O_2.[14,15] The exact crystallographic or molecular structure of the uranium oxides may differ with formation conditions, as proposed here. Melt temperatures of the salts are ∼350, 550, or 770 °C for LiCl−KCl eutectic, pure LiCl, and pure KCl, respectively. Uranium chloride will remain solid up to 837 °C. In this experiment, unexpected uranium oxides formed in the sample, which may remain solid-phase well over 1000 °C. This then presents a temperature range during reactor operation where uranium oxide precipitates could exist in the molten fuel salt; this is essential to understand and mitigate for reactor operation. The aim of this study is to identify, via both X-ray absorption fine structure (XAFS) and Raman spectroscopy, the common uranium oxide phase observed at high temperatures and to describe its formation mechanisms.

2. METHODS

2.1. Sample Preparation. Anhydrous lithium chloride (LiCl) and potassium chloride (KCl) were obtained from BeanTown Chemicals with a supplier-reported cation mass fraction purity of >99.9%; uranium trichloride (UCl_3) was obtained from TerraPower without a purity specification. The purity of the alkali chlorides and UCl_3 was estimated by evaluation of the DSC-determined melting point and peak shape, as well as through confirmation of structure by room-temperature powder X-ray diffraction (XRD). Early Raman measurements confirmed the initial presence of pure UCl_3. The melting points of LiCl and KCl were determined as 606.6 ± 1.4 and 771.4 ± 1.7 °C, respectively, where temperature uncertainties are expanded uncertainties $U(T)$. UCl_3 also had a single peak, although broader than those of the alkali chlorides, at 832 ± 4.9 °C. More details about these measurements and material characterization can be found in a previous work.[16]

Samples were prepared within an MBraun Unilab Pro glovebox under high-purity argon with H_2O and O_2 concentrations maintained below 3 and 10 ppm, respectively. Salts were weighed on an Ohaus PA84C scale with ±0.3 mg precision, and a total mixed mass of at least 100 mg was used to minimize uncertainties in composition. To ensure a homogeneous mixture, the samples were manually ground in an agate mortar and pestle for 15 min. Samples were then sealed within Netzsch 100 μL stainless steel crucibles with a custom Ni liner by appropriately torquing metal screw top/threads. The SS crucibles were loaded in a larger SS crucible and then sealed inside the glovebox.

Once the loading process was finished, the large crucibles were removed from the glovebox and loaded into a box furnace, where they were subjected to mechanical agitation for 30 min at 100 °C above the expected liquidus temperature followed by rapid quenching in water and subsequent annealing at 450 °C for 6 h, as previously described.[16]

The molar ratio of the mixed salts was determined by inductively coupled plasma-optical emission spectrometry (ICP-OES, PerkinElmer Avio 200) for digested samples, as shown in Table 1. A solution of 5% v/v of HNO_3 from the High-Purity Standards (HPS) was used as a blank for the ICP-OES as well as a solvent for each sample, which is dissolved with the Ni liner to avoid any sample loss by a microwave digester (Titan MPS 16 Position, T_{max} = 175 °C, 20 bar, for 10 min), and the solutions are diluted to a measurable range. Li, K, and U compositions were calibrated with five different concentrations + blank (0, 1, 2.5, 5, 7.5, and 10 ppm).

2.2. XAFS Spectroscopy. The XAFS experiments were performed at Stanford Synchrotron Radiation Lightsource (SSRL), Beamline 11-2. The sample sits within a heater consisting of a ceramic heating element inside a copper jacket, while water is pumped through an outer channel providing insulative cooling. Temperature calibration was done using a K-type thermocouple to relate temperature and voltage using a fourth-order polynomial fit. This heater design was used previously in *in situ* X-ray experiments for model salts.[17,18] Samples were transferred from original Ni-lined crucibles to a BN crucible sealed with a mechanical screw top and placed in bags inside an argon glovebox. These BN crucible samples were shipped in sealed plastic bags and moved to atmosphere at the time of data collection, spanning anywhere from 0 to 72 h.

Measurements were performed across the U L3 edge at 17166 eV. An yttrium foil is placed behind the sample, and the energy space is calibrated to the Y K-edge, 17034 eV. X-ray absorption near edge structure (XANES) and extended X-ray absorption fine structure (EXAFS) spectra were recorded by scanning the energy of the incident beam from 240 eV below the L3 edge (E_0 − 240 eV) to 800 eV above the L3 edge (E_0 + 800 eV) and recording the change in intensity of the beam at the ion chambers before and after the sample (i.e., transmission mode). The XAS spectra were recorded in trans-

https://doi.org/10.1021/acs.jpcb.4c02776
J. Phys. Chem. B 2024, 128, 11174−11185

mission mode at room temperature, at select temperatures up to 800 °C, as well as at 25 °C after the sample resolidified. At each temperature step, the heater temperature was allowed to equilibrate for 30−40 min. Sample crucibles were exposed to the atmosphere for anywhere from a few hours to a few days depending on the sample; this variance was not expected to be significant and hence was not a target parameter in the experimental design.

For sample 5, the same energy range of 240 eV below to 800 eV above the L3 edge is used, but the data are instead collected at room temperature only in fluorescence mode to a 100-element XRF detector located perpendicular to the beam. Absorption mode was not possible for S5 due to the high concentration of uranium, resulting in high beam attenuation.

2.3. Raman Spectroscopy. In an atmosphere-controlled glovebox (<1 ppm of O_2 and H_2O), each sample aliquot was loaded into its specially made BN crucible (7 mm OD, 6 mm ID, 3 mm deep; Stanford Materials). To safeguard against cross-contamination, a new crucible was used for each experiment. The sample-loaded crucible was put into a Linkam TS1500 high-temperature stage, which was subsequently sealed to minimize atmospheric exposure during either transport or measurement. Additionally, the assemblage was placed into a gasket-sealed container before removal from the glovebox. After transporting to the spectroscopy suite, the assemblage was associated with the Raman microscope under continuous argon flow (55 cc/min). Transport and association total time was within 1/2 h.

Raman scattering spectroscopy was conducted with a Horiba LabRAM Evolution Raman spectromicroscope equipped with an 800 mm focal length spectrograph, a cooled back-illuminated deep-depleted 1024 × 256-pixel CCD detector using a 100 mW 532 nm laser with no attenuation, and interchangeable magnification objectives. The confocal hole aperture was set to 200 μm and the grating to 1800/mm. LabSpec software supplied with Raman spectroscopy was used in this work.

Using the Raman microscope, samples were aligned with the laser beam, focused with the macro-objective using an achromatic lens ×50 mm or ×100 mm focal length. The microscopy feature additionally allowed samples to be imaged in their solid and molten states as well as phase-state changes to verify the melting/fusion temperature. Indeed, samples lost structural integrity and liquified at the melting points that had been previously measured with DSC. Measurements at melting-point temperatures saw opaque film formation on the viewing window. This phenomenon necessitated a quicker acquisition window than that of lower temperature spectra (<15 min), which resolved measurement issues.

Application of *in situ* Raman spectroscopy from room to melting point was done while recording nonpolarized spectra for all samples except 100% UCl_3, which was measured at 25 °C only. For quality control assurance and to identify optimal measurement parameters, Raman measurements were taken at room temperature over the range of 80−3800/cm before and after each experimental session. A minimum of two aliquots per sample were measured, if their spectra matched. Each spectrum was corrected by the prerecorded instrument-specific response to a calibrated white light source, namely the intensity correction system. Raman vibrations within 900−90/cm will correlate with uranium in the present samples and contribute to the identification as well as refinement of the local environment.[19−25] Thus, the measured samples are plotted to focus on the 900−90/cm Raman shift regions of interest.

2.4. Computational Approach. The selection of a structure to fit the EXAFS portion of this work was expected to be a solved process to report the coordination number. However, the introduction of oxygen and formation of unplanned molecules created an open-ended question, requiring the authors to consider and select from all potential thermodynamically and chemically favorable compounds. A thorough explanation of the process is given in Section 4.1. It was ultimately determined, through qualitative comparison and successful fits of the data, that the phase seen in the X-ray absorption spectroscopy (XAS) data fit only with a β-U_3O_8 or a γ-UO_3 crystallographic structures.[26−28] EXAFS fits alone do not exclude this γ-UO_3. Bruce Ravel's Artemis within the Demeter XAS package[29] is used to interpret the corresponding CIF files and perform the FEFF calculations. The theoretical scattering peak locations in the R-space of both β-U_3O_8 and γ-UO_3 are presented in Figure 1. Each line represents a

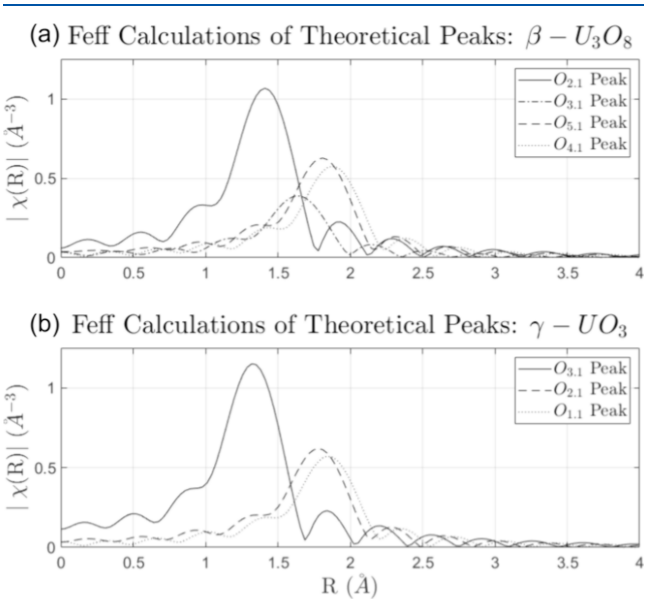

Figure 1. FEFF calculated plots of (a) β-U_3O_8 (room temp) and (b) γ-UO_3 (100 °C) peaks.

signature, in R-space, an unique U−O bond found in the crystal structure. The similarity between the two symmetries of the phases is apparent in the EXAFS data and nearly indistinguishable. However, a UO_3 with a U(VI) oxidation state is expected to decompose if heated in atmospheric O_2 partial pressures[30] and thus not attainable given experimental conditions, even in the worst case of contamination.

3. RESULTS

3.1. XAFS Spectroscopy Results. Raw XAFS data was processed using Athena and was then fitted using Artemis FEFF calculations. Of the nine temperature set points, the highest temperature, 800 °C, exhibits the best fits and convergence of the data sets. Processed XAFS data in *k*-space show clear similarity in the spectra of all 800 °C samples and is presented in Figure SI2 in the Supporting Information document. This convergence is also evident in the oxidation state of the uranium atoms, determined by the XANES region of the spectra. Table 2 presents the white line peaks of the

https://doi.org/10.1021/acs.jpcb.4c02776
J. Phys. Chem. B 2024, 128, 11174−11185

Table 2. XANES White Line Peak Values for Samples 1, 2, 4, and 6

temperature (°C)	S1:5 mol % UCl_3 in LiCl (eV)	S2:5 mol % UCl_3 in KCl (eV)	S4:5 mol % UCl_3 in LiCl-KCl (eV)	S6:20 mol % UCl_3 in KCl (eV)
400	17,169.1	17,168.9	17,169.1	17,169.2
500	17,169.5	17,169.3	17,169.2	17,169.2
550	17,169.5	17,169.2		17,169.2
600	17,169.5	17,169.5	17,169.4	17,169.3
700	17,169.5	17,169.4	17,169.4	17,169.5
800	17,169.4	17,169.4	17,169.4	17,169.5
resolid	17,169.5	17,169.5	17,169.6	17,169.6

XANES region, which converge from a range of 17,165.9–17,168.3 at room temperature[31] to a homogeneous 17,169.4 eV at 800 °C across all samples. An example of how white line peaks are interpreted from the XANES region is shown in Figure 2. The measured beam intensity is recorded as a function of X-ray energy; then, the derivative of this curve is plotted so the maximum absorption peak corresponds to the X-intercept as seen in Figure 2. Uniformity in the white line peaks can be correlated to uniformity in the average oxidation state of uranium in the melt. Thus, for example, it could not follow that some samples are primarily UCl_3 while others are primarily UCl_4.

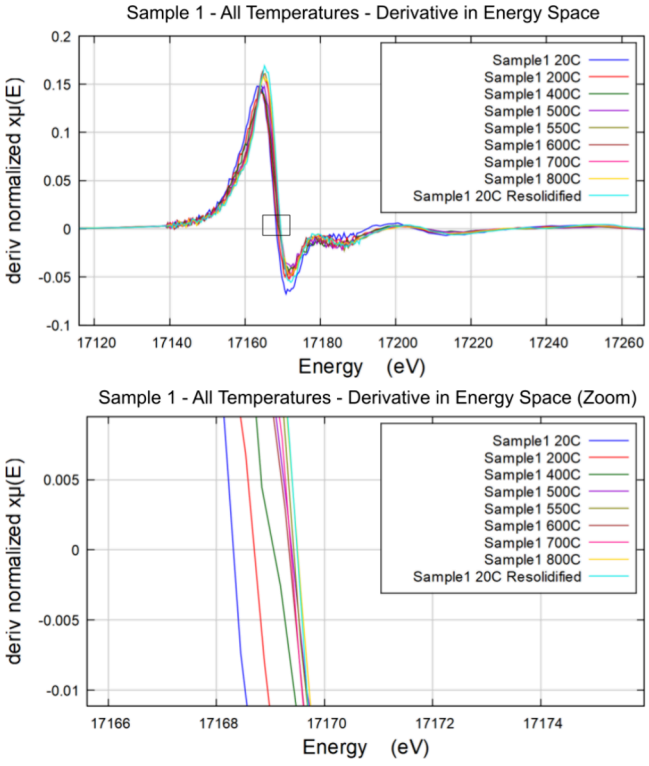

Figure 2. X-ray absorption near edge spectra (XANES) for all sample 1 temperatures.

This convergence of structure in the samples enabled accurate fitting to be completed for the EXAFS results of samples at 800 °C. All fits were completed using the crystallographic structure for β-U_3O_8 and are represented with a dashed line.[26] Results of this data processing and corresponding fits are presented in Figure 3 for the 800 °C spectra and Figure 4 for the solidified spectra. Parameters used to fit the crystallographic structures to the measured data are determined to be reasonable and are presented in Table 3.

3.2. Raman Spectroscopy Results. The measured Raman vibrational frequency bands and corresponding mode assignments for samples S1, S2, S4, S5, and S6 are summarized in Tables SI1–SI5. Figure 5a–e present the Raman spectra with annotated vibrational frequencies. Previously reported molecular vibrational symmetry modes and corresponding vibrational frequencies are detailed in Table SI6.

5 mol % UCl_3 in LiCl (Sample S1). At all measured temperatures, several bands occur in the low vibrational frequency region of the spectrum corresponding to ν(U–Cl) stretching modes as well as lattice and intermolecular vibrations. Raman spectroscopy results for sample S1 are given in Table SI1 and Figure 5a. Additionally, the band at 103/cm corresponds to the vibrational frequency for the translational motions of single uranium atoms. In the high region, S1 expresses a very intense ν_1 symmetric stretching mode. Only the uranyl ion complex ($UO_2^{(2+)}$) and the orthorhombic structure γ-UO_3 have the most intense vibrational frequency band located in this region. Its presence along with that of the midregion 487/cm: $\delta(A_{1g}$ O–U–$O_{(eq)}$, γ-$UO_3)$ strongly suggests that S1 has some symmetry aspects that are similar to that of γ-UO_3, which suggests the U AOS (average oxidation state) may be near U(VI). Additionally, in the current context, the band at ~339/cm corresponds to the symmetric stretching $\nu(A_{1g}$ U–O) in U_3O_8 as well as a bending vibrational mode $\delta(A_{1g}$ O–U–$O_{(eq)})$ in γ-UO_3. A very broad peak spans across the regions from ~215 to 450 punctuated with small intensities correlated with, for instance, a 305/cm specific to U–Cl symmetric stretching vibrations ν(U–Cl) of a U–O–Cl complex. However, a band more specific to the U(5.33) oxidation state of U_3O_8, occurs in the midregion with a doublet band at 641 and 618/cm. Here, at elevated temperatures, arises a weak 638/cm peak, assigned as the $\nu(A_u$ chain O–U–O–U, $U_3O_8)$ mode, while the midregion 485–488/cm band assigned to $\delta(A_{1g}$ O–U–$O_{(eq)}$, γ-$UO_3)$ mode becomes very weak.

In summary, the Raman spectra demonstrate that sample S1 has a higher U AOS, near U(VI) at lower temperatures, which reduces to U(5.33), that of U_3O_8, at elevated temperatures. Note that there is no assertion that the sample is either γ-UO_3 or U_3O_8 but that the sample spectra contain vibrational frequency elements similar to these molecular symmetries.

5 mol % UCl_3 in KCl (Sample S2). Raman spectroscopy results for sample S2 are listed in Table SI2 and Figure 5b. At temperatures ≤400 °C, a doublet band (770 and 740/cm) appears in the high vibrational frequency region. The very intense band in the high region is assigned to $\nu_1(A_{1g}$ U–O, $UO_2^{(2+)}$ of γ-$UO_3)$ for the stretching of O–U–O along the axial direction and corresponding to the AOS of U(VI). With a temperature increase, *until just before the melt*, the high region doublet peak converges into a single band at 770/cm. The S2 uranyl ν_1 bands in the high vibrational frequency region of the spectra have multiple shoulder peaks of much weaker intensity than that of ν_1. The weak shoulders of ν_1 may be assigned to ν(O–U–O, U_3O_8). The midregion bands of the S2 spectra are assigned to the $\nu(E_g$ U–O, $U_3O_8)$ at 489/cm. Both of these characteristics, the weak ν bands in the high vibrational frequency region and the development of the most intense bands occurring in the midregion, correlate with U_3O_8 molecular symmetry, which suggests that at least some fraction of the sample is U(5.33).

https://doi.org/10.1021/acs.jpcb.4c02776
J. Phys. Chem. B 2024, 128, 11174–11185

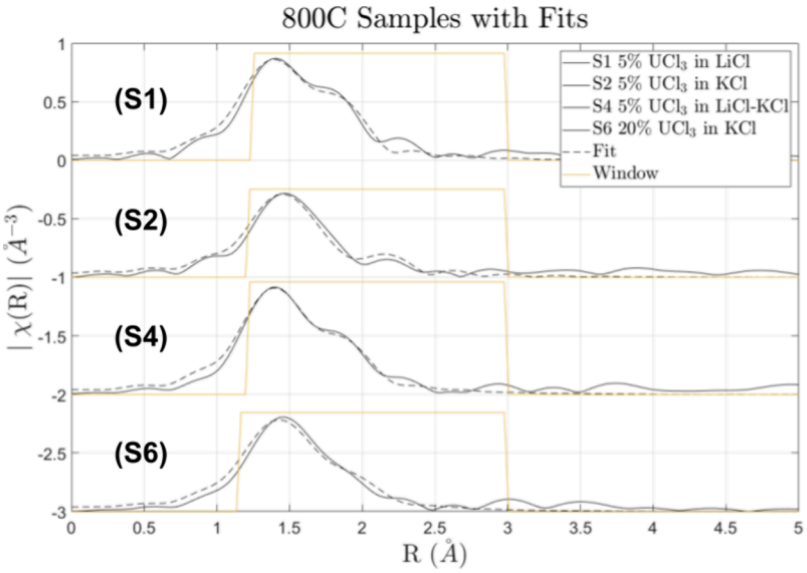

Figure 3. EXAFS scans for samples 1, 2, 4, and 6 at 800 °C with fits using the β-U_3O_8 structure.[26]

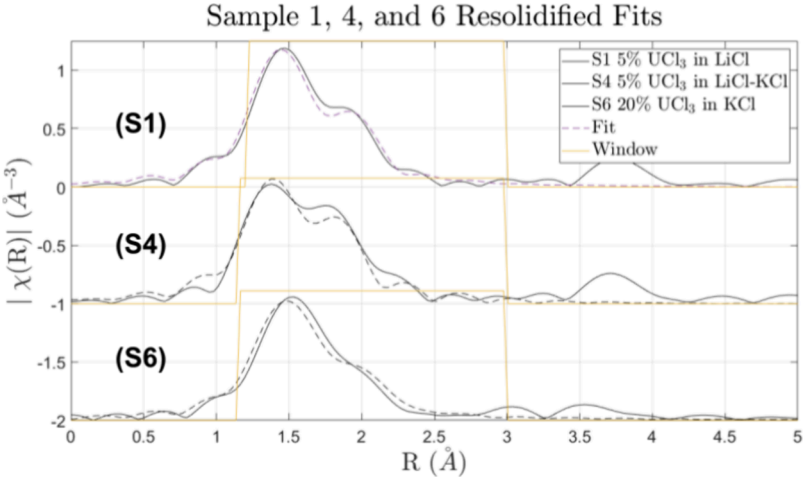

Figure 4. EXAFS scans for samples 1, 4, and 6 at 20 °C resolidified with fits using the β-U_3O_8 structure.[26]

Table 3. EXAFS Fitting Parameters for Samples 1, 2, 4, and 6 at 800 °C Fits

800 °C fitting parameters for β-U_3O_8								
sample composition	**amp**	E_0	R_1(Å)$U-O_{2.1}$	R_2(Å)$U-O_{5.1}$	R_3(Å)$U-O_{4.1}$	σ^2 (10^{-3} Å^2)	**reduced** χ^2	*R* factor
S1 5 mol % UCl_3 in LiCl	0.90	5.2	1.79 ± 0.10	2.27 ± 0.03	2.37 ± 0.00	2.4 ± 0.1	388	0.031
S2 5 mol % UCl_3 in KCl	0.90	7.9	1.85 ± 0.03	2.30 ± 0.01	2.52 ± 0.15	5.3 ± 0.2	98.8	0.030
S4 5 mol % UCl_3 in LiCl-KCl eutectic	0.90	6.6	1.79 ± 0.10	2.27 ± 0.03	2.41 ± 0.04	4.1 ± 0.8	147	0.014
S6 20 mol % UCl_3 in KCl	0.90	6.7	1.80 ± 0.08	2.26 ± 0.04	2.41 ± 0.04	5.1 ± 1.1	1167	0.024

Thus, an U-O complex is present at all temperatures, although it transforms from lower- to higher-temperature corresponding to a decrease in AOS to a final complex based on the molecular symmetry of U_3O_8. Primary features of the Raman spectra are the moderate intensity band assigned to ν(E_g U−O, U_3O_8) at *approx.* 486−494/cm in the midregion and the very intense band in the high region assigned to ν_1(A_{1g} U−O, $UO_2^{(2+)}$ of g γ-UO_3). Overall, these vibrational bands correlate with molecular symmetry aspects of γ-UO_3 as well as U_3O_8, suggesting that the predominant molecular symmetry species of S2 has an AOS between U(5.33 and VI) at lower and moderate temperatures. In the melt, the predominant molecular symmetry corresponds to U_3O_8, suggesting an AOS of or near U(5.33).

To summarize, at temperatures below the melting point, the predominant molecular symmetry of the S2 complex corresponds with both γ-UO_3 and U_3O_8 having an AOS between U(5.33) and U(VI). In the melt, the loss of the very intense band in the high region assigned to ν_1 along with the very weak shoulder bands that remain suggests that the melt has molecular symmetry features of U_3O_8 with a corresponding AOS at or near U(5.33).

5 mol % UCl_3 in Li−K−Cl (Sample S4). Raman spectroscopy results for sample S4 are listed in Table SI3 and Figure 5c. The low vibrational frequency bands of the spectra

https://doi.org/10.1021/acs.jpcb.4c02776
J. Phys. Chem. B 2024, 128, 11174−11185

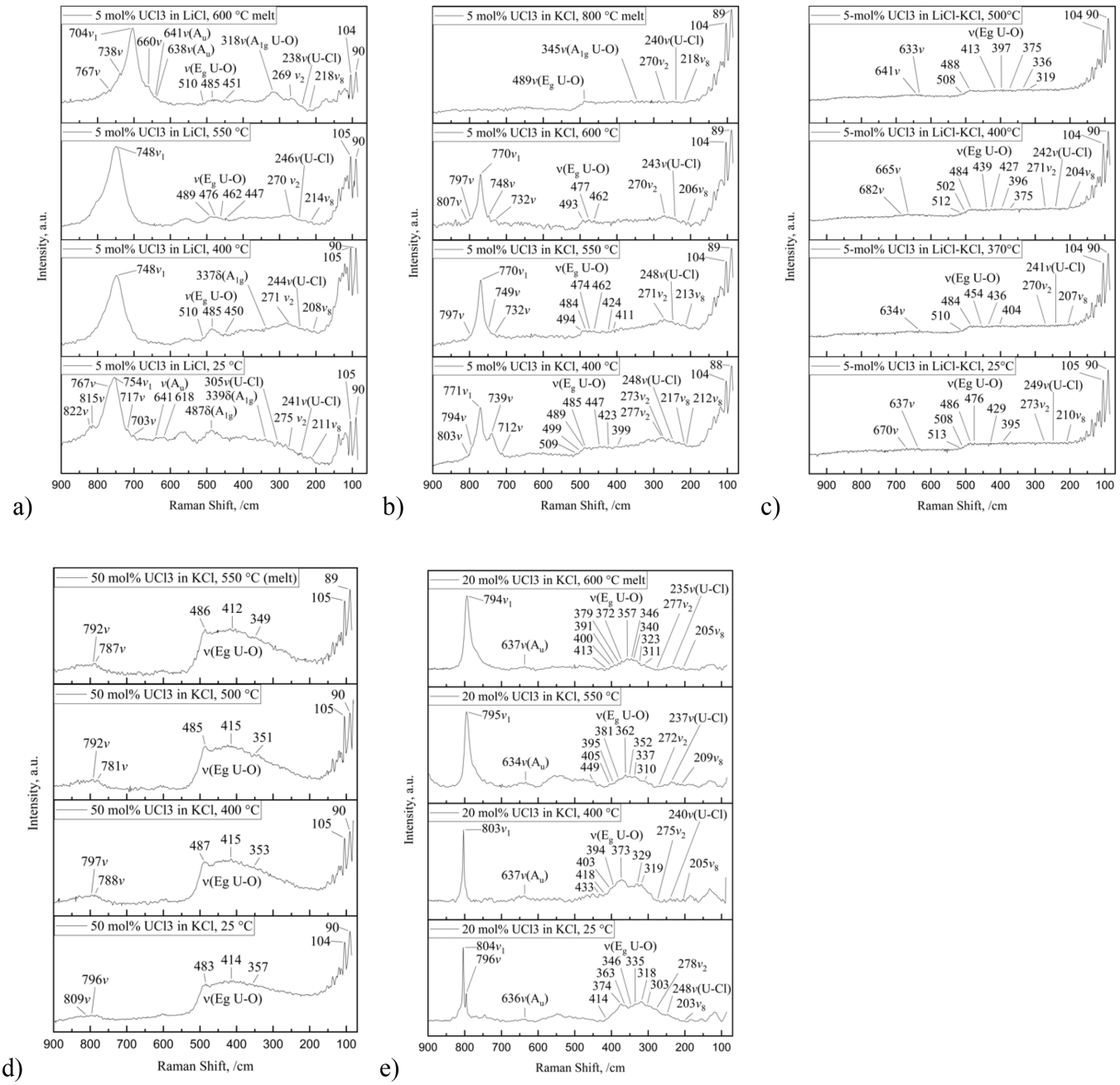

Figure 5. (a−e) Raman spectra of samples (a) S1, (b) S2, (c) S4, (d) S5, and (e) S6, as measured from low temperature to the melt. Notations are used in the plots to assist identification of important vibrational frequency bands and their assigned modes, which correspond to molecular vibrational symmetry aspects of U−Cl and U−O−Cl species as well as γ-UO_3 and U_3O_8. In the plot, the notations ν_1, ν, and $\nu(A_u)$ correspond with the (A_{1g} U−O, $UO_2^{(2+)}$ of γ-UO_3) and ν(O−U−O, β-U_3O_8) symmetric stretching modes and the (A_u chain O−U−O−U, β-U_3O_8) asymmetric stretching mode, respectively. $\nu(E_g$ U−O) represents the midregion fingerprint (E_g U−O, U_3O_8) mode composed of multiple overlapping peaks with some punctuated intensities rising above the broad band. Finally, $\nu(A_{1g}$ U−O), ν_2, ν(U−Cl), and ν_8 correlate with (A_{1g} U−O, U_3O_8), $\nu_2(A_{1g}$ U−Cl_4), ν(U−Cl, $UO_2Cl_4^{(2-)}$), and $\nu_8(E_g$ UO_2Cl_2) vibrational modes, respectively. T(U) corresponds to the vibrational mode for translational motions of single uranium atoms typically reported between 103 and 105/cm. Greater detail about previously reported molecular vibrational symmetry modes and corresponding vibrational frequencies are provided in the Supporting Information (Table SI6).

correlate with U−Cl as well as lattice and interatomic vibrational frequencies. There are numerous overlapping bands spanning the midrange of the spectra. The extensive overlapping of peaks explains the very broad band spanning much of the midregion. The strong band at *approx.* 484−488/cm is the most intense band in the spectrum, which also correlates with the commonly reported spectra of U_3O_8. The vibrational frequency of this band is too high in the spectrum to correspond with one of the hyper-stoichiometric uranium dioxides as the $\nu(T_{2g}$ U−O, $UO_2) \sim 445 \pm 4$/cm for UO_{2+x} ($0 < x < 0.1$). Likewise, the $\nu(E_g$ U−O, $U_3O_8)$ at about 480−485/cm assigned for the 475/cm band of $UO_{2.12}$ in this structure would also require a band at about 749/cm as well as an assigned band $\nu(A_{1g}$ U−O, $U_3O_8)$ at *approx.* 323−335/cm. Thus, S4 is not a U(IV).

https://doi.org/10.1021/acs.jpcb.4c02776
J. Phys. Chem. B 2024, 128, 11174−11185

Weak bands occur in the high vibrational frequency region (Table SI3). The weak 638/cm peak assigned to the $\nu(A_u$ chain O−U−O-U, $U_3O_8)$ mode may be reasonable for these weak bands in S4. Thus, at all temperatures, for sample S4, the molecular vibrational frequencies have features with similarities to U_3O_8 suggesting that the U AOS is at or near U(5.33). It is of interest that the spectra of the temperature series of S4 and molten S2 have similarities corresponding to molecular symmetry vibrations of U_3O_8.

In summary, the numerous overlapping bands spanning the midregion of the S4 spectra form low-to-melt temperatures with the maximum intensity about 484−488/cm correlate with the $\nu(E_g$ U−O, $U_3O_8)$ mode. Although the S4 spectral features have fairly weak intensity with exception to the sharp low region (U−Cl and lattice vibrations), the midregion wide band with the most intense peak about 484−488/cm correlates with a species with molecular symmetry vibrations like those of U_3O_8 suggesting an AOS at or near U(5.33).

50 mol % UCl_3 in KCl (Sample S5). Raman spectroscopy results for sample S5 are listed in Table SI4 and Figure 5d. The classic U_3O_8 fingerprint bands (Table SI1) in the midregion within a very broad multiplet containing very strong intensity peaks presenting with much overlap are present at all measured temperatures. The high vibrational frequency region of each spectrum has bands ranging from medium to very weak intensity (Table SI3) in the commonly reported band region for the molecular stretching modes engaging the uranyl moiety of U_3O_8. These results correlate very well with those reported by Butler, Allen, Tuan, and others (Table SI6). That the peaks are not strong is typical of the high region for U_3O_8 spectra, as well. The low-region vibrational frequency bands are consistent for the presence of chloride ligands in addition to the expected lattice and interatomic vibrations. The primary phase, which appears to be present at all temperatures, is based on the high region $\nu(O-U-O, U_3O_8)$ and midregion $\nu(E_g$ U−O, $U_3O_8)$ modes corresponding with vibrational bands arising from molecular symmetry aspects similar to those found in U_3O_8. This suggests that the U AOS is close to U(5.33). In summary, the spectra of S5 measured from low-to-melt temperatures have very similar vibrational frequency band features that correlate well with those that arise from U_3O_8 molecular symmetry. This suggests that the AOS is U(5.33) at all temperatures in the S5 sample, 50 mol % UCl_3 in KCl exposed to oxygen.

20 mol % UCl_3 in KCl (Sample S6). Raman spectroscopy results for sample S6 are listed in Table SI5 and Figure 5e. The results of the Raman vibrational frequency band and correlated modes for S6 correspond somewhat with the findings of S2 (Table SI2 and Figure 5b) with a few interesting differences. For S6 at 25 °C, a doublet band appears in the high-frequency vibration region. The very intense band assigned to $\nu_1(A_{1g}$ U−O, $UO_2^{(2+)}$ of γ-$UO_3)$ at about 804/cm correlates with a U AOS of U(6). The second and much weaker band at 796/cm correlates with $v_1(O-U-O, U_3O_8)$ and a U AOS of U(5.33). Additionally, with additional applied temperature and into the melt, the very high intensity band remains. In the midregion, a very broad but strong multiplet occurs centering about the 373/cm instead of the 415/cm[32] as does a very weak band at 636/cm. The former is significantly red-shifted, while the latter has been previously reported for the U_3O_8 molecular symmetry. Bands about the multiplet in the midregion for the U_3O_8 symmetry are very intense, and the broad band comprises several overlapping peaks and contains the v1 band. The band in sample S6 near this position is strong but is not as intense as the band in the high-frequency region, which is more consistent with a Raman spectrum of the γ-UO_3 symmetry. The strong intensity multiplet band in the midregion may be assigned to the $\nu(E_g$ U−O, $U_3O_8)$ mode. Although present at all temperatures, the $\nu(E_g$ U−O) shifts to higher vibrational frequency with temperature as the $\nu_1(A_{1g}$ U−O) of the high vibrational frequency region slightly red-shifts, which is an indication that the U AOS is moving closer to U(5.33) than to U(VI). Moreover, the presence of the 600 s/cm high-frequency band about 630−640/cm is a feature of the antisymmetric stretching mode (A_u) in the O−U−O−U chain. At higher oxidation state (e.g., γ-UO_3 phase), this Raman band would blue-shift to about 690/cm. The band at 600 s/cm is as expected for the U(5.33) oxide.

In summary, the molecular symmetry of S6 at low temperature corresponds primarily as γ-UO_3 but with some symmetry features similar to those of U_3O_8. This suggests an AOS of U(5.33−6) at room temperature. From 400 °C and at temperatures up to just before the melt, the predominant molecular symmetry corresponds to γ-UO_3 with the most intense uranyl band in the high vibrational frequency region. However, the midregion Raman bands demonstrate a strong correlation with U_3O_8 molecular symmetry. Additionally, at temperatures of 550 and molten 600 °C, the bands in the high region corresponding with the $\nu_1(A_{1g}$ U−O) mode slightly red-shift, which suggests that the U AOS is moving closer to U(5.33) than to U(VI).

4. DISCUSSION

4.1. XAFS Spectroscopy. The selection and identification of the β-U_3O_8 phase and exclusion of other phases is presented here. Some further details are provided in Supporting Information Section and Table SI7.

All samples show EXAFS spectra fits that are convergent with similar trends at elevated temperatures (800 °C). This convergence indicates that a similar phase is being reached across all samples, onset by heating, regardless of salt composition. Identical trends are seen across compositions where the only changed parameter is the KCl, LiCl, or KCl−LiCl eutectic. This indicates that the presence of Li or K is not a factor in X-ray spectra, meaning that neither K nor Li is bonded directly to uranium. This narrows the scope of potential compounds engaged in U bonds to only Cl and the now known O_2 contamination.

The contamination is conservatively assumed as atmospheric oxygen. When running potential fits of the data, CO_2, N_2, O_2, and H_2O were considered. Based on widespread literature, under atmospheric conditions, uranium, like most metals, seems to far prefer oxidizing to reacting with other stable components of air. The only additional effect we expect to occur is hydration, but this is expected to be negligible at the high temperatures examined.[30] From this, there is confidence that whatever exists in the data will be dominated by U−O or U−Cl bonds.

Previous analysis of these samples leads to a clear conclusion that U−Cl bonds exist in lower temperature data and fully decompose by high temperatures (see ref 31 and Figure SI1). The common bond length for U−Cl molecules is typically around 2.7 Å.[33−36] Comparison of reported *R* values in Table 3 showed that they are all in the 2.25 to 2.30 Å range and lack any peaks near this 2.7 Å+ bond length. Rather, this is the expected bond length for U−O bonds. This suggests that any

https://doi.org/10.1021/acs.jpcb.4c02776
J. Phys. Chem. B 2024, 128, 11174−11185

uranium chlorides or oxychlorides do not exist in any substantial quantity during EXAFS of the 800 °C samples. It is noted that at lower temperatures, bonds of U−Cl or U−O−Cl length are present and likely decomposing with increasing temperatures. There may still exist kinetically residual uranium chlorides or oxychlorides, but they are below detectable peak levels.

By excluding the region of the phase diagram where uranium chlorides and oxychlorides exist, we are left with possible compositions of UO_2, U_4O_9, U_3O_8, or UO_3. Of the possible uranium oxides, the only thermodynamically stable compound that generated a reasonable fit was a high temperature, β, variation of the typically observed α-U_3O_8. This β-U_3O_8 was originally reported by Siegel[37] in 1955. The potential methods of forming this phase were minimally studied. It has reportedly been formed by heating α-U_3O_8 to 1350 °C and cooling to 100 °C per day[26] or inducing stress on α-U_3O_8.[38] The unexpected formation in this work under novel conditions (UCl_3, under oxygen exposure, in a molten eutectic) is significant. This identification of the measured sample as β-U_3O_8 affirms an oxygen concentration present of roughly that of atmosphere (21%), which should be assumed for all EXAFS conclusions.

Fits using β-U_3O_8 were successful for all samples, which reached 800 °C (S1, S2, S4, and S6) and are shown in Figure 3. XAFS data of heated S5 was not collected due to limitations of heater design and attenuation length at high uranium concentration, and S3 did not reach 800 °C due to beam time constraints. The general convergence of trends in R-space greatly simplifies the problem, removing much of the complexity that would stem from different salt compositions generating different phases. There is a distinct similarity between the measured EXAFS data and the $O_{2.1}$, $O_{5.1}$, and $O_{4.1}$, uranium oxygen peaks shown in the FEFF calculation of β-U_3O_8 (Figure 1). EXAFS fitting parameters, S_0^2, σ^2, E_0, and R, for corresponding fits are reported for all 800 °C scans in Table 3, and all values are within expected ranges. The quality of the fit is reported in Table 3 as "R-factor" and "Reduced χ^2" both meet reportable standards. Several of the resolidified room-temperature samples also continued to fit the β-U_3O_8 fit (Figure 4), and thus this phase is expected to be somewhat stable at room temperature. For other temperature set points, complete data can be found in Table SI2 in the Supporting Information. No coordination numbers were used in the fits. This is because EXAFS fits are limited by the number of parameters that can be fitted without giving so much freedom that the data is meaningless. This principle made including the coordination numbers for every bond a risk to the reliability of the data. Additionally, the uranium oxide formed is not expected to be molten at measured temperatures; thus, solving for the uranium second coordination in the melt would not be reliable.

Table 2 shows that the white line peak of the X-ray absorption near edge spectra (XANES) is stable at high temperatures, and the trend is convergent across all samples. Energy space was calibrated using the yttrium K-edge of a reference foil, 17,038.4 (keV). This white line peak relates to the absorption edge energy and reflects the oxidation state of the uranium atoms. A constant edge energy and average oxidation state (AOS) indicates that all samples are trending to the same phase under heating. The relationship observed for β-U_3O_8 with an AOS of U(5.33+) was found to have a uranium L3 absorption edge of 17,169.4 eV, which shifted from the typical 17,166.0 eV U L3 edge energy.

4.2. Raman Spectroscopy. Although a brief summary is provided here to serve the discussion, a detailed application of the prior art in our analyses of the Raman spectra is provided in Table SI6, and the references therein. Interpretations of the Raman data correlate well with those of the EXAFS fits for uranium chloride salt mixtures measured from room-to-melt temperatures. Raman vibrational frequencies were evaluated based on the prior art spanning more than half a century reported by notable Raman spectroscopists. From these reports, the most relevant features of Raman spectra containing U−O, U−O−Cl, and U−Cl bands can be readily and briefly summarized but must then be very carefully applied to spectra that have not previously been reported as uranium molten salts since they are exceedingly complex and do not lend themselves to simple interpretation.

The characteristic (and noted as "true") vibrational band of fluorite structure UO_2, having O_h symmetry, is 445/cm. The presence of a 1150/cm band is often observed, although it is not expected based on molecular symmetry. Due to the temperature dependence of this 1150/cm band position, its presence is due to *electronic scattering rather than a phonon process* . The triplet feature across 300−500/cm is typically used as a fingerprint in U_3O_8[32,38,39] and is often identified with a multiplet of at least seven vibrational modes.[40] Typically, *three approximately* 335, 400, and 475/cm (±15/cm) *bands with much overlap* and one band about 750−810/cm correspond to U_3O_8.[32,38] The broad 700−500/cm is detected in U_4O_9/U_3O_7, corresponding with the increasing uranium oxidation state, and while the characteristic 1150/cm band of the UO_2 fluorite structure disappears, the 445/cm band yet remains.[38] That the characteristic $UO_{(2+x)}$ spectrum features the same two bands as stoichiometric UO_2 but include a broad band in the 700−500/cm range was independently reported elsewhere by He and Shoesmith.[41] An intense symmetric stretching band at 870/cm correlates with pure $UO_2^{(2+)}$uranyl ion at room temperature, although the introduction of subsequent increase in chlorinity was shown to red-shift the uranyl vibrational band.[42,43] Conversely, ref 44 reported the uranyl ν_1 band in molten LiCl-KCl mixtures will blue-shift with increasing LiCl/KCl. However, the work of Dargent and colleagues[42] further demonstrated with the use of an uranyl complex in a noncompeting ionic background matrix of 0.01 M UO_2NO_3 solution (no salt matrix) that the ν_1(U−O) vibrational frequency band blue-shifted positively with temperature and conversely did red-shift under a similarly applied temperature increase when exposed to a salt matrix of increasing LiCl content as a function of the increasing chlorinity.

Of further note, all previously cited Raman spectroscopy studies were applied at temperatures significantly below those of the melt for uranium chloride salt mixtures. The present study is the first to apply Raman spectroscopy to examine uranium chloride salt mixtures from room to melt temperatures. The effect of temperature has been noted as similar in the current work to that of the prior art up to the temperatures reported therein. However, in the present work, we have demonstrated that as the temperature increases and approaches that of the melt, the formation of β-U3O8 occurs and becomes the predominant phase and thankfully does so thermodynamics dictate. Yet, kinetics also plays a role during this formation as evidenced by the presence of lingering U−O−Cl molecular symmetry aspects present in weak vibrational

https://doi.org/10.1021/acs.jpcb.4c02776
J. Phys. Chem. B 2024, 128, 11174−11185

frequency bands of some samples in the Raman data, which are not observable in the EXAFS fits. This is readily explainable.

For samples S1, S2, S4, and S6, Raman spectroscopy was able to identify the phase transformation of γ-UO_3 to U_3O_8 at elevated temperatures and in the melt. The reduction in U AOS from primarily U(VI) to one nearer to U(5.33+) was demonstrated by the red shift of high vibrational frequency bands along with the formation of midregion "U_3O_8 fingerprint" bands. Sample S5 was identified as U_3O_8 from room temperature into the melt, which demonstrated the presence and stability of the U_3O_8 phase across all measured temperatures for this sample.

Several bands are present in the low vibrational frequency region of the spectra of S1, S2, S4, S5, and S6, which correspond to ν(U−Cl) stretching modes as well as lattice and intermolecular vibrations. Of note, these low-frequency vibrational modes are common features reported for the Raman spectra of metal-halide systems as well. That the U−Cl stretching modes are present in samples S1, S2, S4, and S5, but not S6 in the solid and liquid phase states is important, as explained below. In the present case, an additional band (103−105/cm) is attributed to the translational mode of single U atoms, which indicates the presence of defects or disorder. These could break the molecular symmetry to allow translational vibrations to couple to other vibrational modes and become Raman active. This finding warrants future work and theoretical calculations to complement the experimental observations of the Raman activity of uranium atom translational motions in this context.

As a function of the temperature, the local environment of the uranium changes. Raman spectra can differ between solid and liquid phases due to changes in atomic arrangement and interactions. In a solid, the atoms are in a fixed lattice, and their motions are constrained, resulting in sharper and more defined Raman bands. In a liquid or melt, there is more freedom of movement, which may lead to bands that are broader or shifted from those of the solid state. A change in vibrational frequency as well as a change in the shape of the band indicates a change in the bonding environment. In terms of the bands belonging to U−Cl stretching modes, if vibrational frequencies that are present in the solid state continue to appear in the molten or liquid state, this indicates that the related bond environment has remained intact. This cannot be stated too strongly, as it is important to the intended application for these molten salt materials. If unchanging vibrational frequency bands corresponding to the U−Cl bonds are present in both solid and liquid phases, then the interaction might be strong and consistent across these phase states. Uranium bonding environment persistence might be crucial for MSRs, where stability across different conditions is desired.

However, there is a caveat to this interpretation that some small amount of U−O−Cl bonding environment might linger at elevated temperatures, where phase diagrams indicate that β-U_3O_8 is the more thermodynamically stable phase among those that might be present in these molten salt mixture systems. Typically, Raman data are collected within minutes. Because of the technique requirements, EXAFS measurements are held at target temperatures during measurements for a longer period than those of Raman spectroscopy. The techniques simply have different requirements in this respect. If it is a time difference that accounts for the observation of weak vibrational frequency bands corresponding to molecular symmetry aspects of U−O−Cl phases in the Raman data that were not significantly observable in the EXAFS fits, then this may be, and likely is, a kinetic effect. An alternative explanation is that the increased duration of the EXAFS experiments may have occurred with some small content of oxygen incorporating into the samples. Indeed, even under the exceedingly well-controlled environment of the Raman setup, we did demonstrate in an additional experiment (data not shown here) that after the setup remained under experiment conditions and continuous Ar flow that oxygen did find its way into the sample after 72 h. None of our Raman measurements remained on the instrument this long, of course, as the complete set of measurements on each of these samples was easily completed within 24−48 h.

In addition to temperature effects, an increase in the halide saturation may lead to changes in the U−Cl bonding environment. Raman bands related to new vibrational modes or interactions with the U−Cl may appear, or the intensities of bands may change as a consequence of the addition of greater content of a metal-halide (LiCl, KCl). Either due to a direct interaction with the Li or K cations or to changes in the crystal or melt structure, the U−Cl-associated Raman bands may shift. In the present work, at all concentrations of UCl_3 in KCl with the exception of S6 (20-mol %), the low-frequency region Raman bands did not shift or change shape appreciably, which suggests persistence of the uranium bonding environment across phase states and compositions in the presence of KCl. As stated in the summary above, Fujii et al. reported on the effect of increasing chlorinity on uranium molten LiCl−KCl mixtures from room to 150 °C, which were observable in the uranyl ν_1(U−O) band as an increasing blue-shift.[44] However, Dargent and colleagues[42] initially used a noncompeting ionic background matrix of 0.01 M UO_2NO_3 solution in which to examine the effects of temperature on a uranyl complex and observed a corresponding blue-shift in ν_1(U−O) vibrational frequency that changed positively with temperature, which then under similarly applied temperature increase did red-shift when as a function of the increasing chlorinity in a LiCl salt matrix. Thus, it is reasonable to interpret that the effect of KCl is to blue-shift the U−Cl band and thereby overcome the drive for these bands to red-shift with temperature.

Conversely, in the LiCl case, the bands of this region are very broad and overlapping. Likewise, the oxygen-exposed sample of 20 mol % UCl_3 in KCl had significantly overlapped bands in the low-frequency region. The former may be due to the decreased polarizability of the Li atoms relative to that of the K atoms. The latter may be attributable to lower pure U−Cl content due to a greater amount of sample reacting with oxygen as compared with samples S2, S4, and S5, although why the sample with greater UCl_3 content (50 mol % UCl_3 in KCl, or sample S5) did not respond similarly is of further interest. One might consider the assertions regarding this last example as pure conjecture until review of the Raman data for a sample of the pure 20 mol % UCl_3 in KCl, which had not been exposed to oxygen. In the non-O_2-exposed sample of S6, all low-frequency vibrational bands corresponding to the U−Cl stretching modes were present, sharp, and intense. Moreover, the bands in this latter system did not shift with increasing temperature, much like those of the 5 mol % UCl_3 in KCl. This indicated a U−Cl bonding environment that is stable in KCl at this composition under the measured conditions. It provides an interesting comparison to the oxygen-exposed sample.[31]

https://doi.org/10.1021/acs.jpcb.4c02776
J. Phys. Chem. B 2024, 128, 11174−11185

5. CONCLUSIONS

Alkali chloride salt compositions containing various UCl_3 concentrations in LiCl, KCl, and LiCl−KCl eutectic were investigated. Samples were heated to 800 °C and cooled to room temperature with measurements performed at selected temperatures. XAFS and Raman spectroscopy studies were used to examine the compounds formed, and uranium−oxygen bond lengths and symmetries were observed in the samples before, during, and after heating.

A qualitative analysis of the XAFS spectroscopy data indicates that at high temperatures, >400 °C, there are little to no signature peaks in R-space that would relate to U−Cl bonds. Despite the experimental design to exclude oxygen from the samples and system, clear signatures of U−O bonds are observed. As the samples reach higher temperatures, specifically the 800 °C maximum temperature set point, the trends converge and the EXAFS fits of β-U_3O_8 become more accurate. Thermodynamics and fitting trials and process of elimination by EXAFS fitting rules out nearly any other compound that could exist within this system. XANES data relating the white line peak of the X-ray spectra to the absorption edge, which is a function of the average oxidation state, is also steady with increasing temperature. The edge energy of 17,169.4 eV, which is reported for all samples, is then related to the U(5.33) oxidation state of β-U_3O_8. Lower temperatures show a much higher variation in edge energy likely due to a lower AOS, potentially U(III) or U(IV) as UCl_3, UO_2, or some oxychloride phase. With heating, the AOS increases and the uranium compound within the sample is shown to rapidly shift to a uniform, stable β-U_3O_8 structure. The formation at high temperature and stability through solidification is consistent with the conditions reported by previous works, including the source of the molecular structure used in EXAFS fits.[26]

Raman vibrational frequencies in the S1, S2, and S6 samples correlate with molecular symmetry characteristics of β-U_3O_8 and γ-UO_3 having a U AOS at or near 5.33 to 6.0, when measured at low temperatures (≤400 °C). At higher temperatures, the U AOS increased until eventually reaching the stable β-U_3O_8 phase at an AOS of U(5.33). By contrast, at all measurement temperatures for S4 and S5 as well as the molten S2, vibrational frequencies were consistent primarily with β-U_3O_8 molecular symmetry, indicating that S4 and S5 began at an AOS of U(5.33) and persisted. Additionally, the spectra contain Raman bands consistent with those reported for vibrational modes that correspond to bonding environments of U−O−Cl complexes, although not directly comparable with previously examined uranyl chloride complexes as those studies used purely U(VI) uranyl centers. The Raman spectroscopy measurements and XAFS studies correlate well, indicating that the initially unknown oxygen phases and contamination concentrations were resolved accurately.

The relevance of these conclusions can be distilled to a few points. Uranium chloride and oxychloride will readily give up their Cl, even in the presence of chlorine salts, to fully oxidize. There is a correlation between the resultant product/rate of reaction and temperature of the bulk salt. Samples were run sequentially, meaning regardless of the time they had sat in atmosphere, each began as an oxychloride mixture only fully evolving into β-U_3O_8 when heated to >500 °C. Additionally, the resulting discrepancy of crystal structure between standard α-U_3O_8 and the measured β-U_3O_8 is due in some part to the Cl presence. It is suspected that this is due to the U-Cl breaking down at far lower temperatures than those needed to overcome UO_2 stability.

The identification of a mechanism in which the UCl_3 complex can initially oxidize into a precipitant compound whose melt temperature is much higher provides a significant example for MSR development. This is especially relevant given that the sample mixture is meant to emulate MSR bath chemistry. Identifying the structure of the formed compound and the conditions it formed can help in mitigating any contamination and adverse effects.

■ ASSOCIATED CONTENT

Supporting Information

The Supporting Information is available free of charge at https://pubs.acs.org/doi/10.1021/acs.jpcb.4c02776.

Raman spectroscopy tables, detailed Raman literature summary, EXAFS parameter tables, and additional EXAFS fits (PDF)

■ AUTHOR INFORMATION

Corresponding Author

Wilson K. S. Chiu − *School of Mechanical, Aerospace and Manufacturing Engineering, University of Connecticut, Storrs, Connecticut 06369-3139, United States;* orcid.org/0000-0001-7402-4951; Email: wchiu@engr.uconn.edu

Authors

Benjamin W. Tuffy − *School of Mechanical, Aerospace and Manufacturing Engineering, University of Connecticut, Storrs, Connecticut 06369-3139, United States*

Nancy R. Birkner − *Department of Materials Science and Engineering, Clemson University, Clemson, South Carolina 29634-0901, United States*

Juliano Schorne-Pinto − *Nuclear Engineering Program, University of South Carolina, Columbia, South Carolina 29208, United States;* orcid.org/0000-0003-4208-4815

Ryan C. Davis − *Stanford Synchrotron Radiation Lightsource, SLAC National Accelerator Laboratory, Menlo Park, California 94025, United States*

Amir M. Mofrad − *Nuclear Engineering Program, University of South Carolina, Columbia, South Carolina 29208, United States*

Clara M. Dixon − *Nuclear Engineering Program, University of South Carolina, Columbia, South Carolina 29208, United States*

Mina Aziziha − *Nuclear Engineering Program, University of South Carolina, Columbia, South Carolina 29208, United States;* orcid.org/0000-0003-4001-6413

Matthew S. Christian − *Nuclear Engineering Program, University of South Carolina, Columbia, South Carolina 29208, United States;* orcid.org/0000-0002-3416-413X

Timothy J. Lynch − *School of Mechanical, Aerospace and Manufacturing Engineering, University of Connecticut, Storrs, Connecticut 06369-3139, United States*

Maxwell T. Bartlett − *School of Mechanical, Aerospace and Manufacturing Engineering, University of Connecticut, Storrs, Connecticut 06369-3139, United States*

Theodore M. Besmann − *Nuclear Engineering Program, University of South Carolina, Columbia, South Carolina 29208, United States*

Kyle S. Brinkman − *Department of Materials Science and Engineering, Clemson University, Clemson, South Carolina 29634-0901, United States;* orcid.org/0000-0002-2219-1253

Complete contact information is available at: https://pubs.acs.org/10.1021/acs.jpcb.4c02776

Author Contributions

#B.W.T. and N.R.B. co-first authors.

Notes

The authors declare no competing financial interest.

■ ACKNOWLEDGMENTS

The authors are grateful for the support of Nuclear Energy University Program of the US Department of Energy Award ID: DE-NE0008772, 18-15065: "in situ Measurement and Validation of Uranium Molten Salt Properties at Operationally Relevant Temperatures." Portions of this research were carried out at the Stanford Synchrotron Radiation Lightsource, a national user facility operated by Stanford University on behalf of the U.S. Department of Energy, Office of Basic Energy Sciences. Uranium trichloride was provided by TerraPower. Special thanks are given to Doug Van Campen and Marcia Torres at SLAC National Accelerator Laboratory for assistance in setting up the heater at SSRL and handling of the samples, respectively.

■ REFERENCES

(1) Williams, D. F.; Britt, P. F. *Technology and Applied R&D Needs for Molten Salt Chemistry: Report for the US Department of Energy*; Office of Nuclear Energy Molten Salt Chemistry Workshop, 2017.

(2) *OECD Nuclear Energy Agency on behalf of the Generation IV International Forum, Technology Roadmap Update for Generation IV Nuclear Energy Systems*, 2014.

(3) Okamoto, Y.; Akabori, M.; Itoh, A.; Ogawa, T. X-ray absorption study of molten uranium chloride system. *J. Nucl. Sci. Technol.* **2002**, *39*, 638−641.

(4) Li, X.; Song, J.; Shi, S.; Yan, L.; Zhang, Z.; Jiang, T.; Peng, S. Dynamic fluctuation of U^{3+} coordination structure in the molten LiCl-KCl eutectic via first principles molecular dynamics simulations. *J. Phys. Chem. A* **2017**, *121* (3), 571−578.

(5) Wang, S.; Xiao, S.; Hu, W.; Deng, H. Effect of MCl_3 (M = La, U or Sc) component on the local structures and transport properties of LiCl−KCl−MCl_3 eutectic: A molecular dynamics study. *Electrochim. Acta* **2019**, *306*, 366−376.

(6) Dai, J. X.; Zhang, W.; Ren, C. L.; Han, H.; Guo, X. J.; Li, Q. N. Molecular dynamics investigation on the local structures and transport properties of uranium ion in LiCl-KCl molten salt. *J. Nucl. Mater.* **2018**, *511*, 75−82.

(7) Song, J.; Shi, S.; Li, X.; Yan, L. First-principles molecular dynamics modeling of UCl_3 in LiCl-KCl eutectic. *J. Mol. Liq.* **2017**, *234*, 279−286.

(8) Kosog, B.; la Pierre, H. S.; Denecke, M. A.; Heinemann, F. W.; Meyer, K. Oxidation state delineation via U L III-edge XANES in a series of isostructural uranium coordination complexes. *Inorg. Chem.* **2012**, *51* (14), 7940−7944.

(9) Liu, Y. L.; Yuan, L. Y.; Zheng, L. R.; Wang, L.; Yao, B. L.; Chai, Z. F.; Shi, W. Q. Confirmation and elimination of cyclic electrolysis of uranium ions in molten salts. *Electrochem commun* **2019**, *103*, 55−60.

(10) Cordfunke, E. H. P.; Kubaschewski, O. The thermochemical properties of the system uranium—oxygen—chlorine. *Thermochim. Acta* **1984**, *74* (1−3), 235−245.

(11) Martynova, N. S.; Vasil'kova, I. V.; Susarev, M. P. Thermographic investigation of UO_2, UCl, and KCl ternary and binary systems. *Soviet Atomic Energy* **1965**, *18* (6), 777−783.

(12) Grenthe, I.; Sandino, M. C. A.; Puigdomenech, I.; Rand, M. H. Corrections to the Uranium Nea-TDB Review. *Chemical Thermodynamics of Americium* **1995**, *2*, 347−374.

(13) Smirnov, M. V.; Komarov, V. E.; Koryushin, A. P. Decomposition of uranyl chloride and its interaction with uranium dioxide in molten NaCl-KCl. *Soviet Atomic Energy* **1967**, *22* (1), 34−37.

(14) Volkovich, V. A.; Mehj, I.; Charnock, Dzh. M. X-ray and electronic absorption spectra of uranium in LiCl melt; Rentgenovskie i ehlektronnye spektry pogloshcheniya urana v rasplave LiCl. *Rasplavy* **2004**, 76−85.

(15) Volkovich, V. A.; Ivanov, A. B.; Ryzhov, A. A.; Mal'tsev, D. S.; Shchetinskii, A. V. Reaction of Oxygen with Uranium Trichloride in Molten Alkali Metal Chlorides. *Russian Metallurgy (Metally)* **2021**, *2021* (8), 1040−1043.

(16) Yingling, J. A.; Schorne-Pinto, J.; Aziziha, M.; Ard, J. C.; Mofrad, A. M.; Christian, M. S.; Dixon, C. M.; Besmann, T. M. Thermodynamic measurements and assessments for LiCl-NaCl-KCl-UCl_3 systems. *J. Chem. Thermodyn.* **2023**, *179*, No. 106974.

(17) Kiss, A. M.; Harris, W. M.; Nakajo, A.; Wang, S.; Vila-Comamala, J.; Deriy, A.; Chiu, W. K. S. In Situ Heater Design for Nanoscale Synchrotron-Based Full-Field Transmission X-Ray Microscopy. *Microscopy and Microanalysis* **2015**, *21* (2), 290−297.

(18) Lynch, T. J.; Birkner, N. R.; Christian, M. S.; Wrubel, J. A.; Schorne-Pinto, J.; Van Veelen, A.; Bargar, J. R.; Besmann, T. M.; Brinkman, K. S.; Chiu, W. K. S. In Situ Determination of Speciation and Local Structure of NaCl-$SrCl_2$ and LiF-ZrF_4 Molten Salts. *J. Phys. Chem. B* **2022**, *126* (7), 1539−1550.

(19) Marlow, P. G.; Russell, J. P.; Hardy, J. R. Raman scattering in uranium dioxide. *Philos. Mag.* **1966**, *14* (128), 409−410.

(20) Shamir, J.; Silberstein, A. The Laser-Raman Spectrum of Solid Uranium Hexachloride. *Spectrosc. Lett.* **1971**, *4* (10−11), 341−342.

(21) Allen, G. C.; Crofts, J. A.; Griffiths, A. J. Infrared spectroscopy of the uranium/oxygen system. *J. Nucl. Mater.* **1976**, *62* (2−3), 273−281.

(22) Graves, P. R. Raman microprobe spectroscopy of uranium dioxide single crystals and ion implanted polycrystals. *Appl. Spectrosc.* **1990**, *44* (10), 1665−1667.

(23) Lin, D. H. M.; Manara, D.; Varga, Zs.; Berlizov, A.; Fanghänel, Th.; Mayer, K. Applicability of Raman Spectroscopy as a Tool in Nuclear Forensics for Analysis of Uranium Ore Concentrates. *ract* **2013**, *101* (12), 779−784.

(24) Ho, D. M. L.; Jones, A. E.; Goulermas, J. Y.; Turner, P.; Varga, Z.; Fongaro, L.; Fanghänel, T.; Mayer, K. Raman Spectroscopy of Uranium Compounds and the Use of Multivariate Analysis for Visualization and Classification. *Forensic Sci. Int.* **2015**, *251*, 61−68.

(25) Palacios, M. L.; Taylor, S. H. Characterization of Uranium Oxides Using *in Situ* Micro-Raman Spectroscopy. *Appl. Spectrosc.* **2000**, *54* (9), 1372−1378.

(26) Loopstra, B. O. The structure of β-U_3O_8. *Acta Crystallographica Section B Structural Crystallography and Crystal Chemistry* **1970**, *26* (5), 656−657.

(27) Loopstra, B. O.; Taylor, J. C.; Waugh, A. B. Neutron powder profile studies of the gamma uranium trioxide phases. *J. Solid State Chem.* **1977**, *20* (1), 9−19.

(28) Herak, R. The crystal structure of the high temperature modification of U_3O_8. *Acta Crystallographica Section B Structural Crystallography and Crystal Chemistry* **1969**, *25* (12), 2505−2508.

(29) Ravel, B.; Newville, M. ATHENA, ARTEMIS, HEPHAESTUS: data analysis for X-ray absorption spectroscopy using IFEFFIT. *J. Synchrotron Radiat* **2005**, *12*, 537−541.

(30) Thein, S. M.; Bereolos, P. J., "*Thermal Stabilization of 233UO2, 233UO3, and 233U3O8*." Rep. No. ORNL/TM-2000/82; Oak Ridge National Laboratory: Oak Ridge, TN.

(31) Tuffy, B. W.; Birkner, N. R.; Schorne-Pinto, J.; Davis, R. C.; Mofrad, A. M.; Dixon, C. M.; Aziziha, M.; Christian, M. S.; Lynch, T. J.; Bartlett, M. T.; et al. Identification and Decomposition of Uranium Oxychloride Phases in Oxygen-Exposed UCl_3 Salt Compositions. *J. Phys. Chem. B* **2023**, *127* (27), 6091−6101.

(32) Pointurier, F.; Marie, O. Identification of the Chemical Forms of Uranium Compounds in Micrometer-Size Particles by Means of Micro-Raman Spectrometry and Scanning Electron Microscope. *Spectrochim Acta Part B At Spectrosc* **2010**, *65* (9−10), 797−804.
(33) Servaes, K.; Hennig, C.; van Deun, R.; Görller-Walrand, C. Structure of $[UO_2Cl_4]^{2-}$ in acetonitrile. *Inorg. Chem.* **2005**, *44* (22), 7705−7707.
(34) Wilkerson, M. P.; Burns, C. J.; Paine, R. T.; Scott, B. L. Synthesis and crystal structure of $UO_2Cl_2(THF)_3$: A simple preparation of an anhydrous uranyl reagent. *Inorg. Chem.* **1999**, *38* (18), 4156−4158.
(35) Taylor, J. C.; Wilson, P. W. The structure of uranium(iii) trichloride by neutron diffraction profile analysis. *Acta Crystallographica Section B Structural Crystallography and Crystal Chemistry* **1974**, *30* (12), 2803−2805.
(36) Nazarchuk, E. V.; Siidra, O. I.; Krivovichev, S. V. Crystal Chemistry of Uranyl Halides containing mixed $(UO_2)(X_MO_N)_5$ bipyramids (X = Cl, Br): Synthesis and crystal structure of $CS_2(UO_2)(NO_3)Cl_3$. *Z. Naturforsch., B* **2011**, *66* (2), 142.
(37) Siegel, S. The Crystal Structure of Trigonal U_3O_8. *Acta Crystallogr.* **1955**, *8* (10), 617−619.
(38) Manara, D.; Renker, B. Raman spectra of stoichiometric and hyperstoichiometric uranium dioxide. *J. Nucl. Mater.* **2003**, *321* (2−3), 233−237.
(39) Allen, G. C.; Butler, I. S.; Tuan, N. A. Characterisation of Uranium Oxides by Micro-Raman Spectroscopy. *J. Nucl. Mater.* **1987**, *144* (1−2), 17−19.
(40) Miskowiec, A.; Niedziela, J. L.; Spano, T. L.; Ambrogio, M. W.; Finkeldei, S.; Hunt, R.; Shields, A. E. Additional complexity in the Raman spectra of U_3O_8. *J. Nucl. Mater.* **2019**, *527*, No. 151790.
(41) He, H.; Shoesmith, D. Raman Spectroscopic Studies of Defect Structures and Phase Transition in Hyper-Stoichiometric UO_{2+x}. *Phys. Chem. Chem. Phys.* **2010**, *12* (28), 8108.
(42) Dargent, M.; Dubessy, J.; Truche, L.; Bazarkina, E. F.; Nguyen-Trung, C.; Robert, P. Experimental study of uranyl(VI) chloride complex formation in acidic LiCl aqueous solutions under hydrothermal conditions (T = 21 C−350 °C, Psat) using Raman spectroscopy. *European Journal of Mineralogy* **2014**, *25* (5), 765−775.
(43) Nguyen Trung, C.; Begun, G. M.; Palmer, D. A. Aqueous Uranium Complexes. 2. Raman Spectroscopic Study of the Complex Formation of the Dioxouranium(VI) Ion with a Variety of Inorganic and Organic Ligands. *Inorg. Chem.* **1992**, *31* (25), 5280−5287.
(44) Fujii, T.; Uda, T.; Iwadate, Y.; Nagai, T.; Uehara, A.; Yamana, H. Raman Spectroscopic Study of Uranyl Complex in Alkali Chloride Melts. *J. Nucl. Mater.* **2013**, *440* (1−3), 575−579.

https://doi.org/10.1021/acs.jpcb.4c02776
J. Phys. Chem. B 2024, 128, 11174−11185